Avoiding Undesirable Solutions of Deep Blind Image Deconvolution

Antonie Brožová[1,2] and Václav Šmídl[2]

[1]*Faculty of Nuclear Sciences and Physical Engineering, Czech Technical University in Prague, Czech Republic*
[2]*Institute of Information Theory and Automation, Czech Academy of Sciences, Czech Republic*

Keywords: Blind Image Deconvolution, Deep Image Prior, No-Blur, Variational Bayes.

Abstract: Blind image deconvolution (BID) is a severely ill-posed optimization problem requiring additional informa-
tion, typically in the form of regularization. Deep image prior (DIP) promises to model a naturally looking
image due to a well-chosen structure of a neural network. The use of DIP in BID results in a significant perfor-
mance improvement in terms of average PSNR. In this contribution, we offer qualitative analysis of selected
DIP-based methods w.r.t. two types of undesired solutions: blurred image (no-blur) and a visually corrupted
image (solution with artifacts). We perform a sensitivity study showing which aspects of the DIP-based algo-
rithms help to avoid which undesired mode. We confirm that the no-blur can be avoided using either sharp
image prior or tuning of the hyperparameters of the optimizer. The artifact solution is a harder problem since
variations that suppress the artifacts often suppress good solutions as well. Switching to the structural similar-
ity index measure from L_2 norm in loss was found to be the most successful approach to mitigate the artifacts.

1 INTRODUCTION

Recovery of a sharp, clean image from a degraded one
is a difficult task regardless of the type of degradation.
This paper is concerned with blur degradation, which
may be caused by the relative motion of a camera and
a scene, turbulence in the atmosphere, or the focus
of a camera. Assuming a spatially invariant blur, a
blurred image d can be represented as a convolution
(denoted by $\circledast$) of a point spread function (PSF) k and
an underlying sharp image x

$$d = k \circledast x + n, \qquad (1)$$

where n denotes a noise matrix. The deconvolution
is basically an inverse operation to the convolution
with the aim of recovering the sharp image from the
blurred one. The deconvolution is called blind (BID)
when not only the sharp image but also the PSF is
unknown. The task is then to minimize

$$\|d - k \circledast x\|, \qquad (2)$$

with respect to both x and k. To preserve the energy
of the image, k is required to contain only nonnegative
values and sum to 1.

Minimizing (2) is difficult since there can be many
local minima other than the ground-truth solution.
One notable solution is the trivial no-blur solution
reconstructing the observation by the blurred image

and Dirac delta PSF. Therefore, it is necessary to add
some regularizer to (2) or prior information that helps
recover the real sharp image x.

Sharp image priors were designed to yield a higher
probability of sharp images over blurred ones to steer
the optimization algorithm from the no-blur solutions,
starting with (Miskin and MacKay, 2000), (Likas and
Galatsanos, 2004) and (Molina et al., 2006). Vari-
ational Bayes (Tzikas et al., 2009), (Kotera et al.,
2017) and Maximum Aposteriori (MAP) (Levin et al.,
2011), (Perrone and Favaro, 2016) approaches were
mainly discussed and various priors were proposed
(Wipf and Zhang, 2014). Total variation (TV) min-
imizing the L1 norm of horizontal and vertical dif-
ferences of the sharp image was proposed among
first image priors (Chan and Wong, 1998). Later,
the strength of super-gaussian priors (Babacan et al.,
2009) was discovered. Similarly to TV, they assume
that the gradient of the sharp image is sparse and most
of its values is centered around zero. The priors do not
necessarily need to prefer the sharp image but rather
help to avoid the blurred one. Although these tradi-
tional methods are quite successful, their efficiency
depends on a blur type, and inverse operations often
leave the estimates of the sharp images degraded by
artifacts (see the left image in Figure 1).

A completely different approach to blind image
deconvolution is based on deep learning (Huang et al.,

559

2023), (Zhao et al., 2022), (Asim et al., 2020). Supervised deep learning models usually require training on large datasets, giving them more information than the traditional methods get and, therefore, outperforming them. However, there are real-world scenarios where large datasets are not available and for a long time, the Bayesian methods have been state-of-the-art for these problems. In 2018 (Ulyanov et al., 2018) proposed Deep Image Prior (DIP), stating that the structure of a deep neural network is a regularizer of the problem itself. It was shown that such a neural network learns naturally smooth images faster than noise, which, according to (Shi et al., 2022), is caused by faster learning of low-frequency information. They successfully used it for image denoising, inpainting, and superresolution. (Ren and et al., 2020) combined the DIP image network with a feedforward neural network (FNN) representing the PSF in 2020 and proposed SelfDeblur. This model deblurs images without any training dataset and outperforms the Bayesian methods. They also propose to use TV regularization, but unless the images are noisy enough, it has no visible benefit. (Kotera et al., 2021) suggests that its success is not caused only by the DIP, but by some interplay between the structure of the network and the optimizer.

DualDeblur (Shin et al., 2021) utilizes DIP and multiple blurry images. (Wang et al., 2019) focus on the PSF and represent it with DIP as well as the sharp image. (Bredell et al., 2023) combined the DIP with Wiener deconvolution. The two conceptions of the 'prior' have been combined by (Huo et al., 2023), where the DIP-based model was complemented by the sharp image prior and BID solved as minimization of the variational lower bound.

However, all presented methods report only the average PSNR of the restored images without a detailed analysis of the effect of the components of their method. In this contribution, we analyze the effect of selected variations of DIP deblurring to shed some light on their role in the quality of the restoration. Specifically:

1. We demonstrate that DIP-based deconvolution is an intrinsically stochastic process, and thus it can be understood only via statistical methods analyzing full distribution.

2. We focus on two specific types of undesired solutions, the "no-blur" and "artifact" solutions, and propose a PSNR-NB metric to distinguish them.

3. We demonstrate experimentally that the no-blur solution can be avoided by choosing the optimization hyperparameters well or by the sharp image priors.

4. We illustrate that the suppression of the artifact solutions is a much more demanding task and is greatly influenced by the stochasticity of the DIP-based methods. The most significant improvement seems to be brought by switch to SSIM loss during optimization.

2 BACKGROUND AND MOTIVATION

Here, we will shortly review the analyzed methods, demonstrate their stochastic nature, and formulate the research objectives.

2.1 Deep BID Methods

We now introduce the studied algorithms SelfDeblur and VDIP, and a simplification of the SelfDeblur algorithm that reveals some properties of the MAP approach.

SelfDeblur. (Ren and et al., 2020) combines two generative neural networks: $\mathcal{G}_x$ representing x and $\mathcal{G}_k$ representing k. The estimates of x and k are generated by inputting fixed random arrays z_x and z_k, into the networks. $\mathcal{G}_x$ is a 5-level U-net (Ronneberger et al., 2015) with skip connections and bilinear upsampling. $\mathcal{G}_k$ is a FNN with one hidden layer. Softmax at the output of $\mathcal{G}_k$ preserves the L_1 norm of the PSF. The minimized loss is

$$\mathcal{L}_{SDB}(\theta_k, \theta_x) = \text{MSE}(d, \mathcal{G}_k(\theta_k|z_k) \circledast \mathcal{G}_x(\theta_x|z_x)),$$
(3)

where θ_x, resp. θ_k represents the trainable parameters of $\mathcal{G}_x$, resp. $\mathcal{G}_k$. The two networks are optimized jointly in 5000 epochs using Adam optimizer (Kingma and Ba, 2014) with learning rates (LR) $\eta_x = 10^{-2}$ for $\mathcal{G}_x$ and $\eta_k = 10^{-4}$ for $\mathcal{G}_k$. LRs are halved in 2000th, 3000th and 4000th iterations and z_x is perturbed by Gaussian noise with the standard deviation of 0.001 in every iteration. Although not in the original paper, the code provided by authors contains a switch to SSIM loss (5) after 1000 iterations. (Kotera et al., 2021) reported that this switch sometimes causes the optimization to deteriorate, so it will not be used as default in this method.

SimplerSDB. A slightly simpler model is also used in this paper. x is represented by $\mathcal{G}_x$ from SelfDeblur, but k is represented only by an array θ_k normalized by softmax function (denoted as $\sigma(.)$). The deconvolution is then formulated as the minimization of

$$\mathcal{L}_{SSDB}(\theta_k, \theta_x) = \text{MSE}(d, \sigma(\theta_k) \circledast \mathcal{G}_x(\theta_x|z_x)).$$
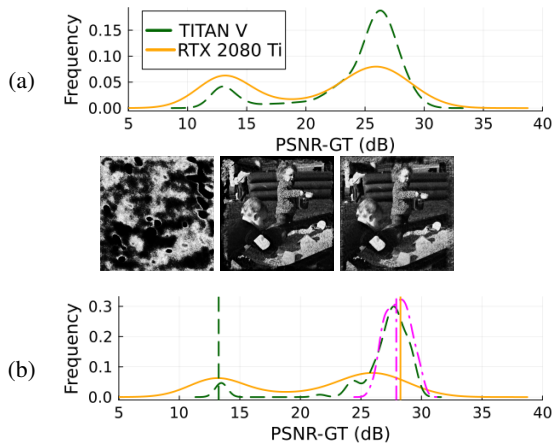(4)

Figure 1: Illustration of stochastic influences. **(a)** PSNR histograms of nondeterministic computations on two GPUs. **(b)** PSNR histograms for three different initial values and nondeterministic computations on NVIDIA GeForce RTX 2080 Ti. The vertical lines show the PSNR of a result obtained by deterministic operations from corresponding initial values. The three reconstructed images are displayed above the graph.

The parameters are again optimized by Adam optimizer and $\eta_k = \eta_x = 10^{-2}$. Random perturbations of z_x and learning rate scheduling used in SelfDeblur are turned off. This algorithm, stripped of everything else but DIP, will be called SimplerSDB.

Variational BID: VDIP. The last algorithm used in this paper for comparison is VDIP (Huo et al., 2023) utilizing two priors for the sharp image: sparse one (VDIP-Sparse) and extreme channel prior (Yan et al., 2017) (VDIP-Extreme). $\mathcal{G}_x$ and $\mathcal{G}_k$ are the same as in SelfDeblur. VDIP not only utilizes the DIP but also adds stronger prior information similar to bayesian methods. Apart from that, the considered loss is MSE-like (3) only in the first 2000 iterations; for the next 3000, it is switched to SSIM (structural similarity index measure) (Wang et al., 2004) loss, which is not mentioned in the paper, but the provided code contains it. The SSIM loss reads as

$$1 - \text{SSIM}\left(d, \mathcal{G}_k\left(\theta_k | z_k\right) \circledast \mathcal{G}_x\left(\theta_x | z_x\right)\right). \quad (5)$$

Furthermore, $\mathcal{G}_x$ is pretrained to reconstruct basic contours in the image and the same scheduling as in SelDeblur is used.

2.2 Stochasticity of BID Algorithms

One issue connecting all three DIP-based algorithms is the stochasticity of their output. It is caused by two factors: i) by initialization of $\mathcal{G}_x$ and z_x, and in some versions also by $\mathcal{G}_k$ and z_k, and ii) by nondeterministic computations on GPU (convolution and
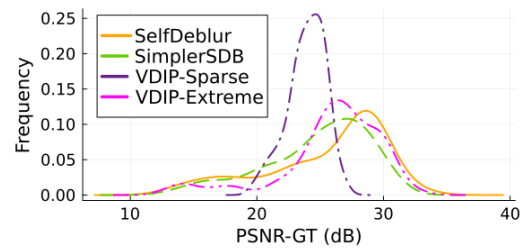

Figure 2: Three runs on the Levin dataset performed by SelfDeblur, SimplerSDB, VDIP-Sparse, and VDIP-Extreme.

Table 1: Mean values of PSNR-GT on three runs on the Levin dataset. SDB denotes SelfDeblur, S-SDB SimplerSDB, VDIP-Sp VDIP-Sparse, and VDIP-Ex VDIP-Extreme.

SDB	S-SDB	VDIP-Sp	VDIP-Ex
26.114 dB	24.792 dB	23.917 dB	25.907 dB

bilinear upsampling). The influence of a GPU is demonstrated by 100 nondeterministic repeated runs of SimplerSDB on NVIDIA GeForce RTX 2080 and NVIDIA TITAN V; one blurred image from the Levin dataset (Levin et al., 2009) was used. Figure 1 (a) shows that there is a significant difference between the two GPUs. The influence of the random initial conditions is demonstrated by 100 runs of SimplerSDB with $\mathcal{G}_x$ with nearest neighbor upsampling for three combinations of initial values of parameters θ_x and the input array z_x on NVIDIA GeForce RTX 2080. Apart from these nondeterministic runs, a deterministic one was carried out for comparison (PyTorch offers a deterministic implementation of convolution); results are displayed in Figure 1 (b). Note that the deterministic computations may lead to a solution very different from the most likely stochastic solution. The three deterministically obtained deblurring results (one for each initial seed) are depicted on the top of Figure 1 (b).

This analysis reveals the sensitivity of SimplerSDB (and inherently all other algorithms based on DIP) not only to stochastic issues such as random initialization but also to computational hardware used in the experiment. This makes a comparison of different methods rather challenging since a naive comparison of novel results with previously published PSNRs may lead to misleading results.

2.3 Evaluation Metrics

The stochasticity of the DIP output is well known, and the majority of publications report average PSNR as a comparison metric. Here, we argue that compressing the whole histogram into a single number removes
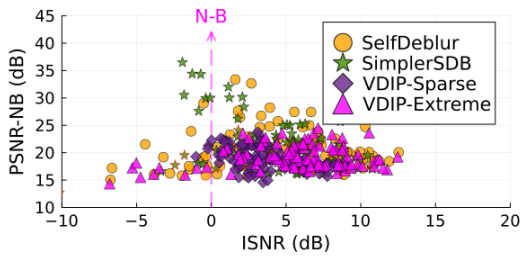
Figure 3: Three runs on the Levin dataset performed by SelfDeblur, SimplerSDB, VDIP-Sparse, and VDIP-Extreme. N-B denotes no-blur.

potentially useful information. This is demonstrated in Figure 2 using the histogram of PSNR (in our paper denoted as PSNR-GT) of the tested algorithms in their default setup on the Levin dataset. The mean values of the PSNR are presented in Table 1.

Since the mean value of the SelfDeblur is the highest, the conventional ranking procedure would select it as the best algorithm. While it offers many high-quality results, it also has many results with very low PSNR. On the other hand, VDIP-Sparse has almost no result with PSNR lower than 20 dB, making it a candidate with a low risk of poor solution. This advantage is compensated by the inability to provide excellent solutions with PSNR greater than 30 dB. An interesting area is around 20 dB PSNR, where VDIP-Extreme has fewer solutions then SelfDeblur. This motivates our search for the nature of these results and analyzing which variation of the method influences them.

2.4 Types of Undesired Solutions

The classical literature on BID extensively discusses two types of undesired solutions: i) the no-blur solution, and ii) an artifact solution. The no-blur solution is an estimate when the image is estimated as the blurred one, and the PSF as the Dirac delta function. The loss value of such a solution is zero when no regularization term is added to (2), so it is certainly a valid solution, yet undesirable. The artifact solution is named after visible artifacts corrupting visually the estimated images. Numerical instability of DIP, which was observed in the original paper, may also generate undesirable solutions. These may be easily detected from the value of the loss function or prevented by learning rate scheduling.

We will focus our attention only on the no-blur and artifact solutions. We introduce a modified metric to visualize this distinction. Specifically, we will compute PSNR not only to the ground truth image, x_{GT}, but also to the blurred image, x_{NB}, formally:

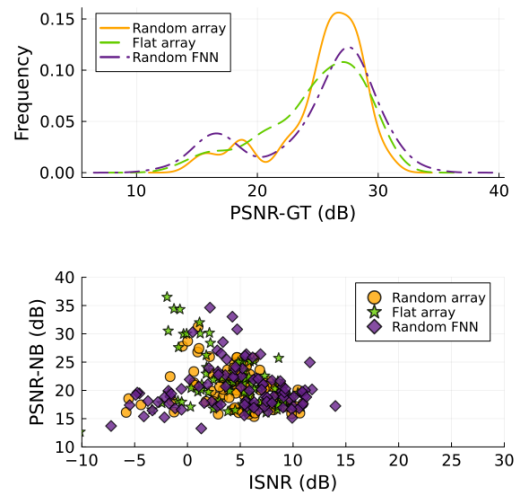$$\text{PSNR-GT}(x) := \text{PSNR}(x, x_{GT}), \qquad (6)$$

Figure 4: The effect of PSF initilization. Flat and random array are results obtained by SimplerSDB, random FNN are generated by SelfDeblur. 3 runs on the Levin dataset.

$$\text{PSNR-NB}(x) := \text{PSNR}(x, x_{NB}). \qquad (7)$$

The no-blur solutions can be recognized by PSNR-NB value around 30 dB. Moreover, when comparing deblurring results on a dataset, it is also useful to measure the improved signal-to-noise ratio, which is defined as

$$\text{ISNR}(x) = \text{PSNR-GT}(x) - \text{PSNR-GT}(x_{NB}).$$

Plotting ISNR and PSNR-NB in 2D space, Figure 3 extends understanding of histogram from Figure 2. It shows that SelfDeblur and VDIP-Extreme are prone to solutions with artifacts that are in the area with low PSNR-NB and negative ISNR. On the other hand, solutions with ISNR around 0 dB and a high value of PSNR-NB show that SimplerSDB and SelfDeblur sometimes reach the no-blur solution. In the subsequent tests, we analyze which variations of the studied algorithms influence these solutions.

3 THE NO-BLUR SOLUTION

3.1 Model and Initialization of PSF

Good initialization is an important part of the MAP approach, such as SelfDeblur. Both the x and k are initialized randomly. In VDIP, an attempt is made to pre-train x towards the blurred image (at least contours) and k to a constant array. We now study the effect of the PSF initialization by various strategies on the SimplerSDB.

Initialization of k as a constant array was found to lead to the no-blur solution more likely than initializing it as a random noise, see Figure 4. On the other
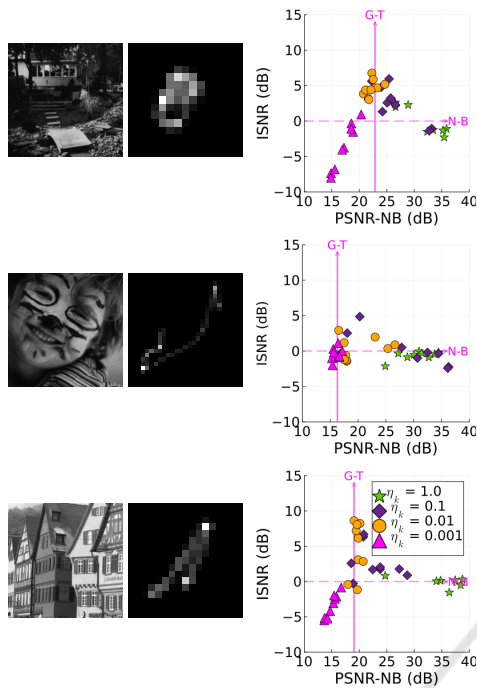
Figure 5: SimplerSDB: Effect of the learning rate η_k. Each scatterplot corresponds to deblurring of one image formed by convolution of the sharp image and the PSF on the left side. Solid vertical line points in the direction of the ground-truth, dashed line in the direction of the no-blur.

hand, random noise leads to solutions with artifacts more often. This holds for both SelfDeblur and SimplerSDB.

Even though neither initialization avoids poor solutions, positive ISNR prevails. We suggest that these two initializations have similar benefits because their character is very distinct from the delta function in the no-blur solution. This hypothesis will be further developed in the next subsection.

Interestingly, there seems to be no big difference between modeling k as FNN and $\sigma(\theta_k)$ only, which contradicts findings from the original paper (Ren and et al., 2020).

3.2 The Setting of the Optimizer

In the case of SelfDeblur and SimplerSDB, the setting of the optimizer plays an important role. We observed that it is necessary to use the Adam optimizer to reach a reasonably low loss value. Firstly, LRs influence whether we find a good, sharp solution or the no-blur solution.

To see the influence, we deblurred 18 images (4 sharp images from the Levin dataset, 2 from the Kodak dataset (kod,) blurred by 3 PSFs from the Levin dataset) with fixed η_x. Since the best choice of η_k de-

pends on the blurred image, Figure 5 shows results for the images separately. It can be seen that higher values of η_k lead the algorithm closer to the no-blur solution. In contrast, too low value of η_k leads to solutions with artifacts if the algorithm converges. This behavior is the same for the other tested images. Therefore, carefully slowing down or speeding up the learning of k may help to avoid the no-blur solution or solution with artifacts. We suggest that this is because the initialization of k is very different from the delta function and a lower speed of learning of k does not allow the algorithm to approach the no-blur solution at the beginning of the optimization. On the other hand, with a higher η_k, the algorithm descends quickly towards the no-blur solution, which the DIP should prefer.

Through hyperparameter search we discovered that increasing the value of β_1^x (hyperparameter β_1 of Adam optimiser of x) helps SimplerSDB avoid the no-blur solution, and the effect is the same for Self-Deblur. The effect that β_1^x has on the whole dataset is shown in Figure 6. We conjecture that this setting helps preserve the original gradient's momentum from the initial optimization stages with constant k, thus avoiding the sharp local minima of the no-blur. In the case of VDIP, there is no obvious difference for the two values of β_1^x, but since VDIP does not generate any no-blur solutions, it is not that surprising.

3.3 Sharp Image Priors

Undeniably, the most effective way to avoid the no-blur is the sharp image prior (sparse and extreme channel) incorporated in the VDIP as can be seen from Figure 3. The variational Bayesian approach seems to be important for DIP models since the TV regularisation did not prove successful (Ren and et al., 2020; Kotera et al., 2021). Moreover, the VDIP algorithm is not sensitive to the choice of the optimizer hyperparameters such as β_1^x studied in Section 3.2.

3.4 Discussion on No-Blur

Mitigation of the no-blur solution has been the objective of the traditional sharp image priors as well as various optimization tricks. It is not any different in the DIP approach. DIP itself does not prefer sharp images, but carefully setting the optimization hyperparameters helps very well to avoid the blurred one. The best option to avoid the no-blur is the combination of DIP with a sharp image prior in VDIP.
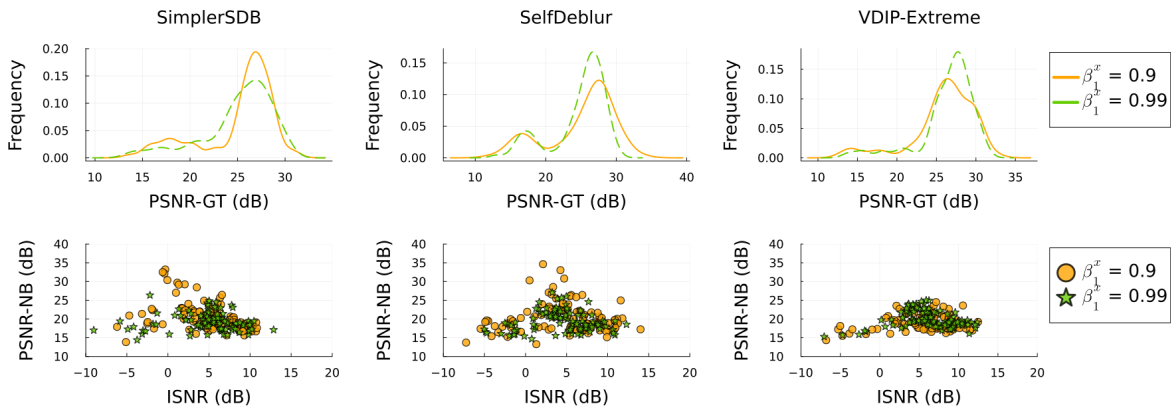
Figure 6: Sensitivity of the solution to the optimizer hyper-parameters β_1^x in terms of PSNR-NB and ISNR for three runs on the Levin dataset.
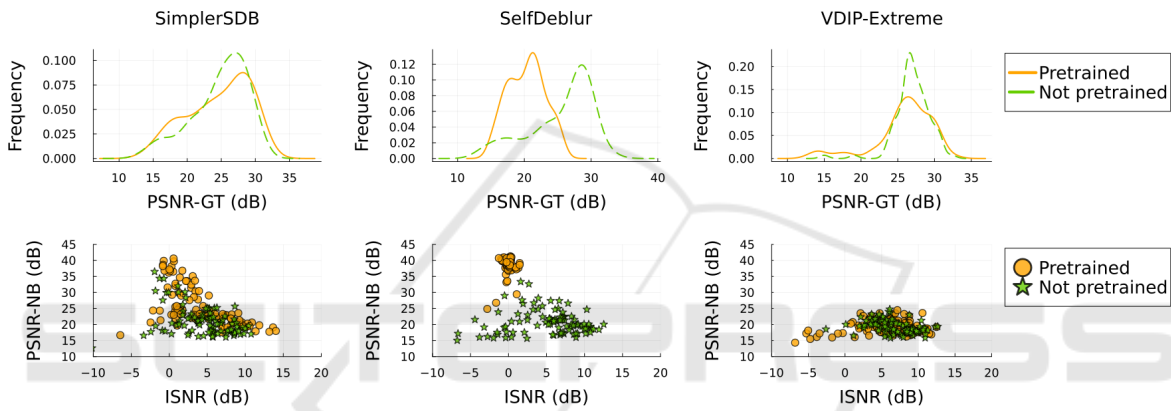

Figure 7: Effect of pretraining on three runs on the Levin dataset.

4 THE ARTIFACT SOLUTION

Solutions with artifacts are generated mostly by Self-Deblur and VDIP-Extreme.

4.1 Sparse Prior

VDIP-Sparse manages to avoid solutions with artifacts, so it can be concluded that the sparse prior minimizing differences between neighboring pixels in the image estimate helps to avoid them. On the other hand, the prior hinders finding estimates with high PSNR-GT. The extreme channel prior does not seem to have this effect.

4.2 Pretraining

VDIP uses pretraining for initialization of both x and k. $\mathcal{G}_x$ is pretrained to return the blurred image, but only in 500 iterations, so it learns only the rough contours of the image. The target for k is the constant array, but after the 500 iterations it still reminds more

of the initial noise. While VDIP-Sparse behaves the same way when the pretraining is omitted, the performance of VDIP-Extreme improves, and it returns fewer solutions with artifacts when pretraining is not used, see Figure 7. The difference could be explained by the extreme channel prior not being as strong as the sparse one and getting lost on the trajectory between the no-blur and sharp solutions.

Since there is no prior in SelfDeblur and SimplerSDB, it could be expected that they will reach more no-blur solutions when pretrained this way. Even though SelfDeblur struggles to reach low loss value, all reconstructions are no-blur solutions. SimplerSDB, on the other hand, does not converge to no-blur in every run. Considering that the main difference here is the model of the PSF, the FNN may learn some information useful for the no-blur during pretraining, causing all reconstructions to be blurred images. The optimizers were not reset after pretraining in this experiment (following how it was done in VDIP), so the moments used in deblurring were those learned on a path toward the blurred image. Simply
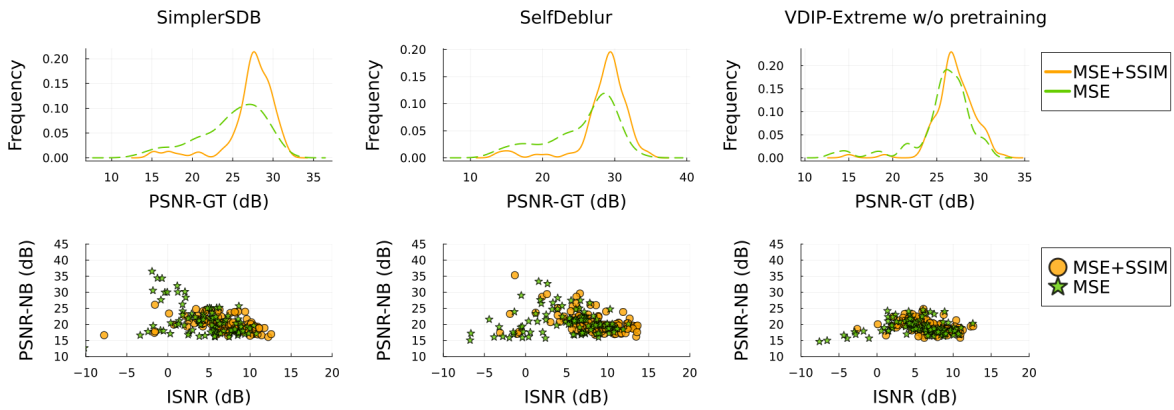
Figure 8: Effect of switching from MSE loss to SSIM loss after 2000 iterations and pretraining on three runs on the Levin dataset.

loading a new optimizer for deblurring in SelfDeblur results in a scatterplot quite similar to the one without pretraining and, surprisingly, containing fewer no-blur solutions. This type of pretraining could work similarly to lowering the learning rate of the PSF. In this case, $\mathcal{G}_x$ starts deblurring closer to the solution, but PSF starts from the same initial point and thus decelerates the learning.

4.3 SSIM Loss

Another algorithmic variation used in VDIP (and the codebase of SelfDeblur) is switching to SSIM loss (5) after 2000 iterations. Figure 8 shows that VDIP-Extreme without pretraining requires the use of the combination of MSE and SSIM loss to avoid solutions with artifacts. When VDIP-Extreme is pretrained, there is no significant effect of the switch and it is the same for VDIP-Sparse (pretrained and not pretrained). In the case of SelfDeblur and SimplerSDB, histograms of PSNR-GT move towards higher values, but some solutions with artifacts remain. Surprisingly, the no-blur solutions are eliminated in the case of SimplerSDB. It is difficult to compare these results because each of these algorithms may be at a different stage of optimization at the time the loss function is switched. Overall, the effect of the SSIM loss is significant and positive, mostly for the variants without a sharp image prior.

4.4 Discussion on Artifacts

Artifacts are not visually plausible, making the resulting solution undesirable. DIP was proven to prefer smoother images, so it could be expected to avoid solutions with artifacts and more likely achieve the no-blur solution. Figure 3 shows that DIP-based models still reach them, and almost none of the tested vari-

ants avoided them. Even though pretraining could be expected to push the algorithms towards smoother solutions, it did not prove to be true. Moreover, pretraining VDIP-Extreme actually hurts its performance. Eventually, the combination of no pretraining and loss with SSIM helped to get rid of the solutions with artifacts. SSIM loss has a positive effect on all the tested algorithms, nevertheless, we cannot conclude that it helps with the solutions with artifacts every time. The only reliable method is the sparse prior in VDIP-Sparse, which eliminates solutions with artifacts at the cost of losing excellent solutions with a lot of details because these images can contain similar intensity changes as those with artifacts.

5 CONCLUSION

The traditional undesirable solutions of blind image deconvolution, i.e. the no-blur solution and the solutions with artifacts, are also present in DIP-based methods. Similarly to the classical methods, the sharp image prior can effectively avoid the no-blur solution. In the case of a variation of a DIP method without a sparse image prior, optimization tricks in the MAP approach can similarly suppress this solution. The solution with artifacts, traditionally attributed to inversions of poorly conditioned matrices, probably is not caused only by this numerical inaccuracy and remains a difficult task for DIP-based method as well. Even though some variations of the method are more prone to this undesirable solution, such as the switch to the SSIM metric, a reliable solution still remains to be found.

ACKNOWLEDGEMENTS

REFERENCES

Kodak image datset. http://r0k.us/graphics/kodak/. Accessed: 2020-01-13.

Asim, M., Shamshad, F., and Ahmed, A. (2020). Blind image deconvolution using deep generative priors. *IEEE Trans Comput Imaging*, 6:1493–1506.

Babacan, S. D., Molina, R., and Katsaggelos, A. K. (2009). Variational bayesian blind deconvolution using a total variation prior. *IEEE Trans Image Process*, 18(1):12–26.

Bredell, G., Erdil, E., Weber, B., and Konukoglu, E. (2023). Wiener guided dip for unsupervised blind image deconvolution. In *2023 IEEE/CVF WACV*, pages 3046–3055.

Chan, T. and Wong, C.-K. (1998). Total variation blind deconvolution. *IEEE Trans Image Process*, 7(3):370–375.

Huang, Y., Chouzenoux, E., and Pesquet, J.-C. (2023). Unrolled variational bayesian algorithm for image blind deconvolution. *IEEE Trans Image Process*, 32:430–445.

Huo, D., Masoumzadeh, A., Kushol, R., and Yang, Y.-H. (2023). Blind image deconvolution using variational deep image prior. *IEEE Trans Pattern Anal Mach Intell*, 45(10):11472–11483.

Kingma, D. P. and Ba, J. (2014). Adam: A method for stochastic optimization. *arXiv preprint arXiv:1412.6980*.

Kotera, J., Šmídl, V., and Šroubek, F. (2017). Blind deconvolution with model discrepancies. *IEEE Trans Image Process*, 26(5):2533–2544.

Kotera, J., Šroubek, F., and Šmídl, V. (2021). Improving neural blind deconvolution. In *2021 IEEE ICIP*, pages 1954–1958. IEEE.

Levin, A., Weiss, Y., Durand, F., and Freeman, W. T. (2009). Understanding and evaluating blind deconvolution algorithms. In *2009 IEEE CVPR*, pages 1964–1971.

Levin, A., Yair, W., Fredo, D., and Freeman, W. T. (2011). Understanding blind deconvolution algorithms. *IEEE Trans Pattern Anal Mach Intell*, 33(12):2354–2367.

Likas, A. C. and Galatsanos, N. P. (2004). A variational approach for bayesian blind image deconvolution. *IEEE Trans Signal Process*, 52(8):2222–2233.

Miskin, J. and MacKay, D. J. C. (2000). Ensemble learning for blind image separation and deconvolution. In *Advances in Independent Component Analysis*, pages 123–141. Springer, London, 1 edition.

Molina, R., Mateos, J., and Katsaggelos, A. K. (2006). Blind deconvolution using a variational approach to parameter, image, and blur estimation. *IEEE Trans Image Process*, 15(12):3715–3727.

Perrone, D. and Favaro, P. (2016). A clearer picture of total variation blind deconvolution. *IEEE Trans Pattern Anal Mach Intell*, 38(6):1041–1055.

Ren, D. and et al. (2020). Neural blind deconvolution using deep priors. In *2020 IEEE/CVF CVPR*, pages pp. 3338–3347. IEEE.

Ronneberger, O., Fischer, P., and Brox, T. (2015). U-net: Convolutional networks for biomedical image segmentation. In *MICCAI 2015*, pages 234–241. Springer, Cham, 1. edition.

Shi, Z., Mettes, P., Maji, S., and Snoek, C. G. (2022). On measuring and controlling the spectral bias of the deep image prior. *International Journal of Computer Vision*, 130:885–908.

Shin, C. J., Lee, T. B., and Heo, Y. S. (2021). Dual image deblurring using deep image prior. *Electronics*, 10(17).

Tzikas, D., Likas, A., and Galatsanos, N. (2009). Variational bayesian sparse kernel-based blind image deconvolution with student's-t priors. *IEEE Trans Image Process*, 18(4):753–764.

Ulyanov, D., Vedaldi, A., and Lempitski, V. (2018). Deep image prior. In *2018 IEEE/CVF CVPR*, pages 9446–9454. IEEE.

Wang, Z., Bovik, A., Sheikh, H., and Simoncelli, E. (2004). Image quality assessment: from error visibility to structural similarity. *IEEE Trans Image Process*, 13(4):600–612.

Wang, Z., Wang, Z., Li, Q., and Bilen, H. (2019). Image deconvolution with deep image and kernel priors. In *2019 IEEE/CVF ICCVW*, pages 980–989.

Wipf, D. and Zhang, H. (2014). Revisiting bayesian blind deconvolution. *Journal of Machine Learning Research*, 15:3775–3814.

Yan, Y., Ren, W., Guo, Y., Wang, R., and Cao, X. (2017). Image deblurring via extreme channels prior. In *2017 IEEE CVPR*, pages 6978–6986.

Zhao, Q., Wang, H., Yue, Z., and Meng, D. (2022). A deep variational bayesian framework for blind image deblurring. *Knowledge-Based Systems*, 249.